A novel electrode with multifunction and regeneration for highly efficient and stable symmetrical solid oxide cell

Yunfeng Tian[a], Yun Liu[b], Lichao Jia[a, c], Aaron Naden[d], Jing Chen[e*], Bo Chi[a, c*], Jian Pu[a, c], John T.S. Irvine[d], Jian Li[a]

[a] Center for Fuel Cell Innovation, School of Materials Science and Engineering, Huazhong University of Science and Technology, Wuhan 430074, China.

[b] China-EU Institute for Clean and Renewable Energy, Huazhong University of Science and Technology, Wuhan 430074, China.

[c] Key Laboratory of Material Chemistry for Energy Conversion and Storage of Ministry of Education, Huazhong University of Science and Technology, Wuhan 430074, China.

[d] School of Chemistry, University of St Andrews, St Andrews, Fife, KY16 9ST Scotland, UK.

[e] School of Chemistry and Chemical Engineering, Henan University of Technology, Zhengzhou, 450001, China.

[*]Corresponding author E-mail: chibo@hust.edu.cn (B. Chi), chj-chs@163.com (J. Chen)

Abstract

Symmetrical solid oxide cells (SSOCs) have been extensively recognized due to their simple cell configuration, low cost and reliability. High performance electrode is the key determinant of SSOCs. Herein, a multifunctional perovskite oxide $La_{0.6}Ca_{0.4}Fe_{0.8}Ni_{0.2}O_{3-\delta}$ (LCaFN) is investigated as electrode for SSOCs. The results confirm that LCaFN shows excellent oxygen reduction reaction (ORR), oxygen evolution reaction (OER), carbon dioxide reduction reaction (CO_2-RR) and hydrogen oxidation reaction (HOR) catalytic activity. In SOFC mode, the SSOCs with LCaFN achieve good electrochemical performance with maximum power density of 300 mW cm^{-2} at 800 °C. For pure CO_2 electrolysis in SOEC mode, polarization resistance of 0.055 Ω cm^2 and current density of 1.5 A cm^{-2} are achieved at 2.0 V at 800 °C. Besides, the cell shows excellent stability both in SOFC mode and SOEC mode. Most importantly, SSOCs with symmetrical LCaFN electrodes show robust and regenerative performance under anodic or cathodic process during the switching gas, showing the great reliability of the SSOCs. The results show that this novel electrode offers a promising strategy for operation of SSOCs.

Keywords: Symmetrical solid oxide cells; $La_{0.6}Ca_{0.4}Fe_{0.8}Ni_{0.2}O_{3-\delta}$; Multifunctional catalyst; Gas switching; Electrochemical performance

1. Introduction

Recently, symmetrical solid oxide cells (SSOCs) with same materials as both the anode and cathode have attracted lots of attention, due to their simple fabrication process and low cost. Moreover, due to existing only one type electrode-electrolyte interface, it can reduce the problem of chemical incompatibility, thermal mismatching, sulfur poisoning and carbon deposition through gas conversion, and therefore these SSOCs are more convenient in practical application [1-5]. In particular, SSOCs provides a way to reduce CO_2 emission by using the intermittent clean energy (wind, solar, tidal energy, etc) to electrolyze CO_2.

An ideal electrode of SSOCs should possess excellent oxygen reduction reaction (ORR), oxygen evolution reaction (OER), CO_2 reduction reaction (CO_2RR) and H_2 oxidation reaction (HOR) catalytic activity. Many materials have been attempted as electrodes for SSOCs' application. The conventional electrode $(La_{0.75}Sr_{0.25})Cr_{0.5}Mn_{0.5}O_3$ (LSCM) was used for a symmetrical solid oxide fuel cell (SSOFC) with good performance, and a peak power density of 300 mW cm^{-2} was achieved at 900 ℃ [6-8]. In addition, electrolysis of CO_2 with the current density 0.18 A cm^{-2} at 2.0 V and 800 ℃ was demonstrated in a symmetrical solid oxide electrolysis cell (SSOEC) with LSCM electrode [9]. Another conventional electrode $Sr_2Fe_{1.6}Mo_{0.5}O_{6-\delta}$ (SFM) was also investigated for SSOFC with peak power density of 835 mW cm^{-2} using H_2 as fuel at 900 ℃ [10]. Hou et al. investigated SFM-SDC as electrodes of SSOEC for H_2O/CO_2 co-electrolysis and the cell can obtained current density of 1.27 A cm^{-2} at 1.6 V and 850 ℃ [11]. Sc doped $La_{0.8}Sr_{0.2}MnO_3$ was introduced as electrodes of SSOFC with peak power density of 310 mW cm^{-2} operated in wet H_2 at 900 ℃ [12]. $Sr_2Ti_{0.8}Co_{0.2}FeO_6$ was also investigated as electrodes of SSOFC with peak power density of 555 mW cm^{-2} at 800 ℃. Besides, other oxides as $La_{0.8}Sr_{0.2}Cr_{0.69}Ni_{0.31}O_{3-\delta}$ [13], $(La_{0.75}Sr_{0.25})(Cr_{0.5}Mn_{0.3}Ni_{0.2})O_{3-\delta}$ [14] $La_{0.5}Sr_{0.5}Ti_{0.75}Ni_{0.25}O_3$ [15], $La_{1.5}Sr_{1.5}Mn_{1.5}Ni_{0.5}O_{7\pm\delta}$ [16] also have been tried as electrodes of SOCs. However, these cells have relative lower electrochemical performance in comparison to the conventional SOFC or SOEC configuration with different anode and cathode [17-19].

Fe-based perovskite oxides have been widely investigated for their many advantages. They are considered to be more stable than Co and Mn based perovskites due to the stable electronic configuration ($3d_5$) of Fe^{3+} [20, 21]. They also have the advantages of better chemical compatibility with $Y_{0.08}Zr_{0.92}O_{2-\delta}$ (YSZ) [22]. Moreover, Fe-based perovskites have matching thermal expansion coefficients (TEC) with YSZ or $Gd_{0.1}Ce_{0.9}O_{2-\delta}$ (GDC), which can enhance the stability of the electrode and electrolyte interface [22, 23]. Fe-based perovskites doped with alkaline-earth metal cations have exhibited good electrochemical performance in SOCs [23, 25, 26]. Bian et al. investigated $La_{0.6}Ce_{0.1}Sr_{0.3}Fe_{0.9}Ni_{0.1}O_{3-\delta}$ as electrodes of SSOFC and the cell

exhibited excellent peak power density of 900 mW cm^{-2} at 850 °C in wet H_2 [27]. $La_{0.4}Sr_{0.6}Co_{0.2}Fe_{0.7}Nb_{0.1}O_{3-\delta}$ electrode-based SSOEC could obtain current density of 0.442 A cm^{-2} at 1.5 V and 800 °C for CO_2 electrolysis [28]. In our previous work, $La_{0.6}Sr_{0.4}Fe_{0.8}Ni_{0.2}O_{3-\delta}$ (LSFN) electrode-based SSOEC could achieve high Faraday efficiency and CO production rate. However, Sr-contained perovskite oxides have a tendency to form $SrCO_3$ causing the irreversible cell performance degradation [3]. $La_{0.6}Ca_{0.4}Fe_{0.8}Ni_{0.2}O_{3-\delta}$ (LCaFN) has been investigated as electrodes for SOFC or SOEC. Nano LCaFN decorated porous doped ceria as an electrode for SSOFC and delivered attractive peak power densities of 510 mW cm^2 at 800 °C using H_2 as fuel [23]. In our previous work, SSOEC with this electrode has a low polarization resistance (0.04 Ω cm^2) and a maximum electrolysis current density (1.41 A cm^2) for pure CO_2 electrolysis at 800 °C and 2.0 V [29]. Due to the ionic radius of Ca^{2+} is smaller than Sr^{2+} and closer to La^{3+}. Doping Ca will result in a stable structure, higher conductivity, matching TEC and chemical compatibility [23, 30, 31]. These aspects are really important for the application in SSOC. However, these cells are all operated in a single mode (SOFC, SOEC), and the redox stability of the cell has not been studied. The systematically investigation of Fe-based perovskites as electrodes for SSOCs almost haven't been attempted yet. In addition, although SSOCs can solve some drawbacks (sulfur poisoning and carbon deposition) due to the switching of working gases for practical application, there is no specific work that has been reported so far on this function.

Herein, a meaningful attempt with "one material for multiple applications" and "one cell for multiple uses" is carried out. The electrocatalytic activity of LCaFN in air, CO_2 and reducing atmosphere, and the electrochemical performance and stability test in SOFC and SOEC mode will be investigated in detail. Furthermore, the stability and robust of SSOCs will be evaluated by switching fuel gas and air alternatively in the same electrode side. Compared with our previous work, this work has truly realized the meaning of symmetrical cells, operating cells by switching gas to achieve stable performance, it is more practical.

2. Experimental

2.1 Sample and cell preparation

The sol-gel method was used to prepare $La_{0.6}Ca_{0.4}Fe_{0.8}Ni_{0.2}O_{3-\delta}$ (LCaFN) powders. $La(NO_3)_3 \cdot 6H_2O$, $Ca(NO_3)_2$, $Fe(NO_3)_3 \cdot 9H_2O$ and $Ni(NO_3)_2 \cdot 6H_2O$ in the appropriate stoichiometric ratios were dissolved in distilled water. Citric acid (CA) and ethylenediaminetetraacetic acid (EDTA) were added in a molar ratio of CA:EDTA:M (metal cations) of 1.5:1:1. The pH value of the above solution was adjusted to 8 by ammonia addition. Finally, the gel was obtained by stirring for 10 h at 80 °C. Then the gel was dried at 200 °C for 5 h and then annealed at 800 °C for 5 h in air to obtain LCaFN powders. GDC was used as the buffer layer and electrode additive.

Electrolyte-supported symmetrical cells were fabricated to test the electrochemical performance of electrodes. GDC paste, pure LCaFN and LCaFN-GDC electrode paste (weight ratio LCaFN:GDC = 6:4) were prepared by grounding the powder with ethyl cellulose in terpineol for 2 h. GDC slurry was first screen-printed on the both surfaces of 300 μm thick YSZ disc (12 mm in diameter) and calcined at 1350 °C for 2 h to form the GDC buffer layer. Then, the electrode was coated onto the electrolyte using the same method, followed by calcination at 1000 °C for 2 h in air (with active area of 0.5 cm^2).

2.2 Characterization and measurements

The crystal structure of materials was characterized by X-ray diffraction (Cu Kα, 40 kV, 30 mA, Shimadzu XRD-7000S). The morphology of samples was characterized by scanning electron microscope (SEM, Sirion 200) and transmission electron microscope (JEOL JEM-2011). The TG curve of samples was measured by TGA (STA449F5, NETZSCH) both under air and 5%H_2/N_2 with a ramping rate of 10 °C min^{-1}. Hydrogen temperature-programmed reduction (H_2-TPR), oxygen temperature-programmed desorption (O_2-TPD) and carbon dioxide temperature-programmed desorption (CO_2-TPD) were examined using our home-made test equipment. For H_2-TPR test, samples were first treated in Ar for 1 h at 350 °C before test.

Then it was conducted from 20 to 950 °C in 5% H_2/N_2. For CO_2 or O_2-TPD test, samples were first treated in pure CO_2 or O_2 at 350 °C for 30 min, and then O_2 or O_2-TPD test was conducted from 20 to 950 °C in Ar. The heating rate and gas flow rate for all tests are 10 °C min^{-1} and 30 mL min^{-1}, respectively. LCaFN bars (24 mm×6 mm×2 mm) were obtained by sintering at 1250 °C for 5 h and the conductivity in air and 5%H_2/N_2 was measured by four-probe method using an Agilent B2901A Precision Source/Measure unit. Thermal expansion coefficient of LCaFN was measured using Thermo Dilation (NETZSCH DIL402C).

For electrochemical performance of electrodes, the symmetrical cells were employed to measure the polarization resistance of LCaFN and LCaFN-GDC electrode in air, H_2 and CO_2. Then they were sealed on an Al_2O_3 tube using ceramic adhesive (552-VFG, Aremco) and Pt current collectors were connected on the surface of each electrode for cell performance test. For SOFC performance test, wet H_2 (50 mL min^{-1}) was fed into one side of the cell and air (50 mL min^{-1}) into another side. For SOEC performance test, one side of symmetrical cell (named obverse side) was exposed to flow pure CO_2 (50 mL min^{-1}) and another side (named reverse side) to stagnant air. The electrochemical tests were recorded using the electrochemical workstation (Zennium IM6 station), including polarization curves (linear sweep rate of 0.01 V s^{-1} from 0 to OCV for SOFC and 0 to 2.0 V for SOEC), electrochemical impedance spectra (EIS) with frequency range of 0.1~10^5 Hz and an amplitude of 10 mV. Stability test was also performed in both SOFC mode and SOEC mode.

3. Results and discussion

3.1. Phase analysis and chemical stability

XRD patterns of the LCaFN powders treated in different atmospheres are presented in Fig. 1 (a). The patterns for the sample treated in air can be well-indexed to $LaFe_{0.75}Ni_{0.25}O_3$ (JCPDS 88-0639). After reduced in 5%H_2/N_2 for 5 h (named R-LCaFN), R-LCaFN still can maintain a stable perovskite structure, which is different to the reduced LSFN [32, 33]. While the

diffraction peaks shift a little towards the lower angles, indicating the expansion of unit cells. This is because the valence of Fe ions changes from a high valence state to a low valence state. The structural stability of LCaFN is also confirmed by TGA as shown in Fig. S1 (see Supplementary material). There are two stages which represent Fe^{4+} to Fe^{3+} at low temperature range and Fe^{3+} to Fe^{2+} corresponding to Ni^{2+} to Ni at elevated temperature range [32]. In addition, R-LCaFN shows a diffraction peak of $FeNi_3$ at 44°, demonstrating the exsolved $FeNi_3$ alloy. Besides, there exists the peak corresponding to CaO after reduction, because the solid solubility of Ca will decrease accompanying the exsolved $FeNi_3$ alloy. When LCaFN was heat-treated in CO_2, the phase structure remains stable, with only some minor peaks of $CaCO_3$ appearing. However, in our previous work [29], these surface $CaCO_3$ particles could be decomposed by simple thermal treatment in air and the electrode could be refreshed to the fresh state. The H_2-TPR curve of LCaFN is measured as shown in Fig. 1 (b), and two main reduction peaks in the range of 100~900 °C can be observed. The first reduction peak α near 400 °C represents the reduction of Ni^{3+} to Ni^{2+}, while another peak β around 700 °C reflects the further reduction of Ni^{2+} to Ni, coupled with a part of reduction of Fe^{3+} to Fe^{2+}. It is consistent with the results of TGA. Compared to $LaFeO_3$ and $La_{0.6}Sr_{0.4}Fe_{0.8}Ni_{0.2}O_3$ [34, 35], LCaFN has a higher reduction peak temperature, which means a more stable perovskite structure. The CO_2-TPD curve of LCaFN is illustrated in Fig. 1 (c). Specifically, the desorption peak below 100 °C represents the physical adsorption of CO_2, and the desorption peak between 200 °C and 300 °C mainly reflects the inherent weak van der Waals forces on the surface of the sample [36]. In the high temperature range, the CO_2 desorption performance is not only related to the oxygen vacancy concentration, but also with the basic sites of the perovskite at high temperature [37,38]. There is a stronger CO_2 desorption peak at around 750 °C than that of LSFN and LFO [3], part of the reason corresponds to $CaCO_3$ decomposition. Indicating the strongly adsorption ability, which may be beneficial for CO_2 electrolysis performance. Fig. 1 (d) displays the O_2-TPD curve of LCaFN. A strong peak at around 600 °C indicates easy generation of oxygen vacancies in

LCaFN, due to the reduction of unstable Fe^{4+} to Fe^{3+} with O_2 desorption. This can facilitate the oxygen surface exchange process [39, 40]. The electronic conductivity of LCaFN in air first increases to reach a maximum of 290 S cm^{-1}, and then gradually decreases with increasing temperature as shown in Fig. 1 (e), which is related to the semiconductor-metal conduction transition of the material [34]. At low temperatures, LCaFN exhibits semiconductor conductive properties. After arriving at a certain temperature, oxygen vacancy defects were continuously formed in LCaFN under high temperature conditions. Formation of an oxygen vacancy will result in decrease in the carrier concentration and thus a decrease in conductivity. In reducing atmosphere, more oxygen vacancies in a reducing atmosphere lead to a lower carrier concentration, thus leading to reduced conductivity. TEC value of LCaFN is only 11.2×10^{-6} K^{-1} as shown in Fig. 1 (f), much closer with GDC (12×10^{-6} K^{-1}) and lower than that of $La_{0.6}Sr_{0.4}Fe_{0.8}Ni_{0.2}O_3$ and those of Co-based perovskites [41, 42].

3.2. Morphology characterization

SEM images of LCaFN and R-LCaFN are shown in Fig. 2. It can be seen that LCaFN powders synthesized by the sol-gel method are fine and uniform, with particle size of around 200 nm (Fig. 2 (a)). EDS of LCaFN in Fig. S2 (b) shows the elements chemical composition of La:Ca:Fe:Ni with 0.624:0.376:0.802:0.198, which is very close to the theoretical stoichiometry. After LCaFN powders being treated in 5% H_2/N_2 for 5 h at 800 °C, many nanoparticles with an average size of 30 nm are uniformly exsolved in-situ on the surface of LCaFN, as shown in Fig. 2 (b, c). EDS mapping and line scanning analysis confirm that the chemical composition of these nanoparticles are Fe-Ni alloy, as shown in Fig. 2 (d, e). This is also consistent with the XRD analysis (Fig. 1(a)). These results prove that LCaFN crystal structure is relatively stable after the reduction and the in-situ exsolved Fe-Ni nanoparticles would be beneficial for the electrochemical performance. It has been confirmed in our previous work and other research groups [32, 33, 39].

The high-resolution TEM image of LCaFN is presented in Fig. 3 (a). The lattice fringe

space of 0.216 nm and 0.153 nm can be indexed to (111) and (211) planes of the perovskite LCaFN. The corresponding EDS mapping of LCaFN shown in Fig. 3 (b) confirms the homogeneous distribution of composition elements. After reduced, the (211) plane of the R-LCaFN has the lattice space of 0.158 nm (Fig. 3 (c)), which is larger than that of LCaFN and it is consistent with the previous analysis of XRD results. This is primarily because Fe^{3+} (0.645 Å) is transformed into Fe^{2+} (0.78 Å) under reducing condition. And Ni^{2+} will transform into metal Ni and in-situ exsolved onto the surface of perovskite oxide. The in-situ exsolved nanoparticles with lattice fringe space of 0.201 nm can be indexed to (111) plane of the $FeNi_3$ alloy. More aggregation of the elements Ni and slight aggregation of Fe also proves this, as shown in Fig. 3 (d).

3.3. Electrochemical performance in SOFC mode

Half-cell performance and SOFC electrochemical performance based on pure LCaFN electrode are shown in Fig. S3-4. It can be seen that LCaFN electrode shows good catalytic activity not only in air, but also in H_2 and CO_2. The polarization resistance (R_p) values in air, CO_2, and H_2 are 0.24, 0.469, and 0.129 Ω cm^2 at 800 °C, respectively, indicating LCaFN electrode possessing the excellent ORR, OER, CO_2-RR and HOR catalytic activity. Furthermore, the electrocatalytic activity of LCaFN has been improved after compositing with GDC as shown in Fig. 4. R_p values in different atmosphere are further reduced as shown in Fig. S5. The power density is improved to 300 mW cm^{-2} and 400 mW cm^{-2} at 800 °C and 850 °C, respectively as shown in Fig. 4 (a). The EIS of the symmetrical cell based on LCaFN-GDC composite electrode measured at different temperatures are shown in Fig. 4 (b). The ohmic resistance values of the cell are found to be 1.443, 0.939, 0.698, and 0.565 Ω cm^2 at 700, 750, 800 and 850 °C, respectively. This is mainly due to the resistance of from YSZ electrolyte (300 μm). Moreover, LCaFN has higher electronic conductivity both in air and 5%H_2/N_2, as shown in Fig. 1 (e). The observed R_p values of the cell are 1.023, 0.385, 0.217 and 0.163 Ω cm^2 in the corresponding temperatures. Interestingly, these values are relatively lower than other reported

results as shown in Table S1. The redox stability of the cell is tested, as shown in Fig. 4 (c). Specifically, the cell is operated in SOFC mode (wet H_2) first at 100 mA cm^{-2} for 30 min at 700 °C, then switched to N_2 purge for 5 min, and finally switched to air for oxidation treatment for 25 min. After 4 cycles, the cell performance remains constantly. In order to test the stability of LCaFN cell performance further, the cell is operated at 750 ° C with higher current density of 250 mA·cm^{-2} and the cell is found to remain stably after 3 cycles. After that, the cell is tested in SOFC mode for a longer time of 35 h at 700 °C with current density of 150 mA cm^{-2} and it can perform stably without any obvious degradation (Fig. 4 (d)). These results prove that LCaFN has good redox stability and robustness.

3.4. Electrochemical performance in SOEC mode

The electrochemical performance of pure CO_2 electrolysis based on LCaFN-GDC composite electrodes is shown in Fig. 5 (a). The current density is found to be raised with increase temperature. The corresponding values are 0.98, 1.5, and 2.25 A cm^{-2} at 750, 800, and 850 °C under 2.0 V, respectively. It shows better performance compared with other reported results as shown in Table S2. The corresponding EIS are shown in Fig. 5 (b). The ohmic resistance values of the cell are 0.989, 0.708, and 0.515 Ω cm^2 at 750, 800, and 850 °C, respectively, similar with the ohmic resistance in SOFC mode. For the polarization resistance, the values are 0.725, 0.621, and 0.43 Ω cm^2 in the corresponding temperature. It is much lower than those reported results as shown in Table S2. According to literature [26, 32, 36], The R_p mainly includes two parts. High frequency part corresponds to charge transfer process (R1) mainly including oxygen ion transportation processes in the electrolyte, electrolyte-electrode interface and the electrodes. The low-frequency part represents the non-charge transfer processes (R2) relate to the electrode surface kinetics, including the transport of CO_2, adsorption of CO_2 and surface diffusion of active species. The simulated results based on the equivalent circuit are listed in Table. S3. Both R1 and R2 gradually decrease with increasing temperature, especially R2 (0.725, 0.621, and 0.43 Ω cm^2), indicating that elevated temperature

accelerates the reduction of CO_2. The EIS of the cell at different voltages are shown in Fig. 5 (c, d). At the low voltage, Higher R_p ascribe to the activation process of the electrode [9]. Once activation is complete. R_p values decrease significantly at the voltage over 1 V, and the reduction of CO_2 also happen at high voltage. Notably, the polarization resistance is only 0.055 Ω cm^2 at 800 °C under 2.0 V. It is much smaller than those reported results as shown in Table S2. These results prove that the LCaFN-GDC symmetrical cell has good CO_2 electrolysis performance.

3.5. Reliability of SSOCs

In order to investigate the reliability of the SSOCs with LCaFN electrodes, the anode and the cathode are fed with CO_2 alternatively. When the gas on both sides of the cell is switched, the electrochemical performance of the cell for CO_2 electrolysis remains almost the same, as shown in Fig. S6. Fig. 6 shows the comparison of electrochemical performance before and after gas switching. The first tested working electrode in CO_2 atmosphere is named the obverse side, and after gas switching, it is named the reverse side. The I-V curves before and after gas switching are shown in Fig. 6 (a). It can be found that the two curves almost overlap. The current density in the reverse side (1.49 A cm^{-2}) is just a little smaller than that in the obverse side (1.51 A cm^{-2}) at 2.0 V at 800 °C, but it is more obvious in the low voltage range. The slight difference of cell performance between the two processes can be attributed to the changes in electrodes. Specifically, electrodes activation process will happen at the low voltage [9, 36]. Once the applied voltage exceeds the initial reduction voltage of CO_2 and the CO_2-RR process will be initiated. In addition, LCaFN electrode will suffer an electroreduction process at the high voltage and then cause a change in bulk diffusion and surface properties of the electrode [43, 44]. At the same time, LCaFN electrode at the other side will start the OER process. The increased oxygen partial pressure may lead to the reduction of oxygen vacancies and the variation of electrode morphology. The LCaFN electrode originally in the CO_2 atmosphere will be exposed to the air after gas switching and then the electrode process on both sides will exchange. Due to the changes of properties on the electrode surface, electrochemical

performance of the cell is slightly affected, especially in the low voltage range. It can be further confirmed by EIS at open-circuit voltage, as shown in Fig. 6 (b). The simulated results are presented in Table. S3. The R_p of the reverse side is a little bit bigger than that of the obverse side, especially R2, which is associated with gas adsorption/desorption, dissociation at the electrode surface. Indicating that the changes of properties on the electrode surface. However, the R_p of the two tests are almost same at working condition, as shown in Fig. 6 (c). It indicates the cell performance is almost stable at working condition after electrodes activation process. The small change in R2 also proves little changes on the electrode surface. Furtherly, the long-term test of the cell is operated by switching the gas, as shown in Fig. 6 (d). The cell can work well during the switching gas. It is worth noting that after each switching, the performance of the cell has a recovery process, which is consistent with our previous study. LCaFN has a self-repairing function [29], because $CaCO_3$ is easy eliminated in the test condition. There is no similar study about SSOCs operated at switching gas. The results open the door for symmetrical cell applications with bright prospects.

3.6. Post-test characterization

After gas switching test, XRD patterns of the LCaFN-GDC electrodes are shown in Fig.7 (a). It can be seen that no new phase exists except LCaFN, GDC and Pt, indicating the stability of the LCaFN phase structure. Moreover, there is no peak of carbon can be found from the Raman spectrum in Fig. 7 (b) [45]. And SEM morphology in Fig. 7 (f) also confirms the absence of carbon deposition on the electrodes. In addition, no electrode exfoliation occurs after test, which proves SSOC with LCaFN electrodes has good structure stability. Furthermore, there is also no element diffusion between the components shown in Fig. S7 and Fig. S8, regardless of gas switching or not.

4. Conclusion

A multifunctional catalyst $La_{0.6}Ca_{0.4}Fe_{0.8}Ni_{0.2}O_{3-\delta}$ perovskite with excellent ORR, OER, CO_2-RR and HOR catalytic activity is synthesized and investigated. The polarization resistance

values in air, CO_2, and H_2 are 0.24, 0.469, and 0.129 Ω cm^2 at 800 °C, respectively. SSOCs with symmetrical LCaFN electrodes can achieve good electrochemical performance with maximum power density of 300 mW cm^{-2} at 800 °C in SOFC mode. While for pure CO_2 electrolysis in SOEC mode, it has a low polarization resistance of only 0.055 Ω cm^2 and achieves a maximum electrolysis current density of 1.5 A cm^{-2} at 2.0 V at 800 °C. Most importantly, SSOCs with symmetrical LCaFN electrodes show excellent robust under anodic or cathodic process, showing the great reliability of the SSOCs. This novel electrode provides a promising strategy for operation of SSOCs.

Author contributions

Yunfeng Tian: Conceptualization, Investigation, Methodology, Writing - Original Draft.

Yun Liu: Investigation, Validation.

Lichao Jia: Formal analysis, Investigation.

Aaron Naden: Investigation, Data Curation.

Jing Chen: Supervision, Data Curation, Review & Editing.

Bo Chi: Supervision, Data Curation, Review & Editing.

Jian Pu: Resources, Investigation.

John T.S. Irvine: Resources, Funding acquisition.

Jian Li: Resources, Funding acquisition.

Declaration of Competing Interest

The authors declare that they have no known competing financial interests or personal relationships that could have appeared to influence the work reported in this paper.

Acknowledgements

We gratefully appreciate for financial support from National Key Research & Development Project (2016YFE0126900), National Natural Science Foundation of China

(51672095, U1910209), and China Scholarship Council (201806160178). The work is also partially supported by State Key Laboratory of Materials Processing and Die & Mould Technology, Huazhong University of Science and Technology (P2019-004). Analytical and Testing Centre of Huazhong University of Science and Technology is appreciated for sample characterizations assistance.

Appendix A. Supplementary data

Supporting Information is available from the Online version at doi: xxxxx .

References

[1] B. Niu, C. Lu, W. Yi, S. Luo, X. Li, X. Zhong, X. Zhao, B. Xu, In-situ growth of nanoparticles-decorated double perovskite electrode materials for symmetrical solid oxide cells, Appl. Catal. B 264 (2020) 118842.

[2] Y. Li, Z. Zhan, C. Xia, Highly efficient electrolysis of pure CO_2 with symmetrical nanostructured perovskite electrodes, Catal.Sci. Technol. 8 (2018) 980-984.

[3] Y. Tian, H. Zheng, L. Zhang, B. Chi, J. Pu, J. Li, Direct electrolysis of CO_2 in symmetrical solid oxide electrolysis cell based on $La_{0.6}Sr_{0.4}Fe_{0.8}Ni_{0.2}O_{3-\delta}$ electrode, J. Electrochem. Soc. 165 (2018) F17-F23.

[4] Y. Zhang, H. Zhao, Z. Du, K. Świerczek, Y. Li, High-performance $smBaMn_2O_{5+\delta}$ electrode for symmetrical solid oxide fuel cell, Chem.Mater. 10 (2019) 3784-3793.

[5] W. Fan, Z. Sun, Y. Bai, K. Wu, Y. Cheng, Highly stable and efficient perovskite ferrite electrode for symmetrical solid oxide fuel cells, ACS Appl. Mater. Interfaces. 26 (2019) 23168-23179.

[6] C. M. Chanquía, A. Montenegro-Hernández, H. E. Troiani, A. Caneiro, A bottom-up building process of nanostructured $La_{0.75}Sr_{0.25}Cr_{0.5}Mn_{0.5}O_{3-\delta}$ electrodes for symmetrical-solid oxide fuel cell: Synthesis, characterization and electrocatalytic testing, J. Power Sources 245

(2014) 377-388.

[7] D. M. Bastidas, S. Tao, J. T. Irvine, A symmetrical solid oxide fuel cell demonstrating redox stable perovskite electrodes, J. Mater. Chem. 17 (2006) 1603-1605.

[8] W. Li, X. Liu, H. Yu, S. Zhang, H. Yu, $La_{0.75}Sr_{0.25}Cr_{0.5}Mn_{0.5}O_{3-\delta}$-$Ce_{0.8}Sm_{0.2}O_{1.9}$ as composite electrodes in symmetric solid electrolyte cells for electrochemical removal of nitric oxide, Appl. Catal. B 264 (2020) 118533.

[9] S. Xu, S. Li, W. Yao, D. Dong, K. Xie, Direct electrolysis of CO_2 using an oxygen-ion conducting solid oxide electrolyzer based on $La_{0.75}Sr_{0.25}Cr_{0.5}Mn_{0.5}O_{3-\delta}$ electrode, J. Power Sources. 230 (2013) 115-121.

[10] Q. Liu, X. Dong, G. Xiao, F. Zhao, F. Chen, A novel electrode material for symmetrical SOFCs, Adv. Mater. 48 (2010) 5478-5482.

[11] S. Hou, K. Xie, Enhancing the performance of high-temperature H_2O/CO_2 co-electrolysis process on the solid oxide $Sr_2Fe_{1.6}Mo_{0.5}O_{6-\delta}$-SDC/LSGM/$Sr_2Fe_{1.5}Mo_{0.5}O_{6-\delta}$-SDC cell, Electrochim. Acta. 301 (2019) 63-68.

[12] Y. Zheng, C. Zhang, R. Ran, R. Cai, Z. Shao, D. Farrusseng, A new symmetric solid-oxide fuel cell with $La_{0.8}Sr_{0.2}Sc_{0.2}Mn_{0.8}O_{3-\delta}$ perovskite oxide as both the anode and cathode, Acta Mater. 57 (2009) 1165-1175.

[13] W. Kobsiriphat1, B. D. Madsen, Y. Wang, M. Shah, L. D. Marks and S. A. Barnett, Nickel- and ruthenium-doped lanthanum chromite anodes: effects of nanoscale metal precipitation on solid oxide fuel cell performance. J. Electrochem. Soc. 157 (2010) B279-B284.

[14] Jardiel T, Caldes M T, Moser F. New SOFC electrode materials: the Ni-substituted LSCM-based compounds $(La_{0.75}Sr_{0.25})(Cr_{0.5}Mn_{0.5-x}Ni_x)O_{3-\delta}$ and $(La_{0.75}Sr_{0.25})(Cr_{0.5-x}Ni_xMn_{0.5})O_{3-\delta}$. Solid State Ionics, 181 (2010) 894-901.

[15] Arrivé C, Delahaye T, Joubert O, Exsolution of nickel nanoparticles at the surface of a conducting titanate as potential hydrogen electrode material for solid oxide electrochemical cells. J. Power Sources, 223 (2013) 341-348.

[16] Vecino‐Mantilla S, Gauthier‐Maradei P, Huvé M, Nickel exsolution‐driven phase transformation from an n=2 to an n=1 Ruddlesden‐Popper manganite for methane steam reforming reaction in SOFC conditions. ChemCatChem, 11 (2019) 4631-4641.

[17] S. Choi, S. Sengodan, S. Park, Y. W. Ju, J. Kim, J. Hyodo, H. Y. Jeong, T. Ishihara, J. Shin, G. Kim, A robust symmetrical electrode with layered perovskite structure for direct hydrocarbon solid oxide fuel cells: $PrBa_{0.8}Ca_{0.2}Mn_2O_{5+\delta}$, J. Mater. Chem. A. 4 (2016) 1747-1753.

[18] C. Yang, Z. Yang, C. Jin, G. Xiao, F. Chen, M. Han, Sulfur‐tolerant redox‐reversible anode material for direct hydrocarbon solid oxide fuel cells, Adv. Mater. 24 (2012) 1439-1443.

[19] S.-L. Zhang, H. Wang, M. Y. Lu, A.-P. Zhang, L. V. Mogni, Q. Liu, C.-X. Li, C.-J. Li, S. A. Barnett, Cobalt-substituted $SrTi_{0.3}Fe_{0.7}O_{3-\delta}$: a stable high-performance oxygen electrode material for intermediate-temperature solid oxide electrochemical cells, Energy Environ. Sci. 11 (2018) 1870-1879.

[20] E. Konysheva, J. T. Irvine, Thermochemical and structural stability of A-and B-site-substituted perovskites in hydrogen-containing atmosphere, Chem.Mater. 21 (2009) 1514-1523.

[21] H. Yokokawa, N. Sakai, T. Kawada, M. Dokiya, Thermodynamic stabilities of perovskite oxides for electrodes and other electrochemical materials, Solid State Ionics, 52 (1992) 43-56.

[22] M. D. Anderson, J. W. Stevenson, S. P. Simner, Reactivity of lanthanide ferrite SOFC cathodes with YSZ electrolyte, J. Power Sources. 129 (2004) 188-192.

[23] G. Yang, C. Su, Y. Chen, M. O. Tadé, Z. Shao, Nano $La_{0.6}Ca_{0.4}Fe_{0.8}Ni_{0.2}O_{3-\delta}$ decorated porous doped ceria as a novel cobalt-free electrode for “symmetrical” solid oxide fuel cells, J. Mater. Chem. A. 2 (2014) 19526-19535.

[24] M.-H. Hung, M. V. M. Rao, D.-S. Tsai, Microstructures and electrical properties of calcium substituted $LaFeO_3$ as SOFC cathode, Mater.Chem. Phys. 101 (2007) 297-302.

[25] J. Li, B. Wei, Z. Cao, X. Yue, Y. Zhang, Z. Lu, Niobium doped lanthanum strontium ferrite

as a redox-stable and sulfur-tolerant anode for solid oxide fuel cells, ChemSusChem. 11 (2018) 254-263.

[26] Y. Song, Y. Chen, M. Xu, W. Wang, Y. Zhang, G. Yang, R. Ran, W. Zhou, Z. Shao, A cobalt-free multi-phase nanocomposite as near-ideal cathode of intermediate-temperature solid oxide fuel cells Developed by Smart Self-Assembly, Adv. Mater. (2020) 1906979.

[27] L. Bian, C. Duan, L. Wang, R. O'Hayre, J. Cheng, K.-C. Chou, Ce-doped $La_{0.7}Sr_{0.3}Fe_{0.9}Ni_{0.1}O_{3-\delta}$ as symmetrical electrodes for high performance direct hydrocarbon solid oxide fuel cells, J. Mater. Chem. A. 29 (2017) 15253-15259.

[28] Z. Yang, C. Ma, N. Wang, X. Jin, C. Jin, S. Peng, Electrochemical reduction of CO_2 in a symmetrical solid oxide electrolysis cell with $La_{0.4}Sr_{0.6}Co_{0.2}Fe_{0.7}Nb_{0.1}O_{3-\delta}$ electrode, J. CO_2 Util. 33 (2019) 445-451.

[29] Y. Tian, L. Zhang, Y. Liu, L. Jia, J. Yang, B. Chi, J. Pu, J. Li, A self-recovering robust electrode for highly efficient CO_2 electrolysis in symmetrical solid oxide electrolysis cells, J. Mater. Chem. A. 7 (2019) 6395-6400.

[30] N. Ortiz-Vitoriano, I. R. de Larramendi, S. N. Cook, M. Burriel, A. Aguadero, J. A. Kilner, T. Rojo, The formation of performance enhancing pseudo-composites in the highly active $La_{1-x}Ca_xFe_{0.8}Ni_{0.2}O_3$ system for IT-SOFC application, Adv. Funct. Mater. 23 (2013) 5131-5139.

[31] N. Ortiz-Vitoriano, C. Bernuy-López, I. Ruiz de Larramendi, R. Knibbe, K. Thydén, A. Hauch, P. Holtappels, T. Rojo, Optimizing solid oxide fuel cell cathode processing route for intermediate temperature operation, Appl. Energy. 104 (2013) 984-991.

[32] S. Liu, Q. Liu, J.-L. Luo, Highly stable and efficient catalyst with in situ exsolved Fe–Ni alloy nanospheres socketed on an oxygen deficient perovskite for direct CO_2 electrolysis, ACS Catal. 6 (2016) 6219-6228.

[33] Y. Tian, L. Zhang, L. Jia, X. Wang, J. Yang, B. Chi, J. Pu, J. Li, Novel quasi-symmetrical solid oxide electrolysis cells with in-situ exsolved cathode for CO_2 electrolysis, J. CO_2 Util. 31

(2019) 43-50.

[34] Y. Tian, W. Wang, Y. Liu, L. Zhang, L. Jia, J. Yang, B. Chi, J. Pu, J. Li, Cobalt-free perovskite oxide $La_{0.6}Sr_{0.4}Fe_{0.8}Ni_{0.2}O_{3-\delta}$ as active and robust oxygen electrode for reversible solid oxide cells, ACS Appl. Energy Mater. 2 (2019) 3297-3305.

[35] K. Zhao, F. He, Z. Huang, A. Zheng, H. Li, Z. Zhao, $La_{1-x}Sr_xFeO_3$ perovskites as oxygen carriers for the partial oxidation of methane to syngas, Chinese J. Catal. 35 (2014) 1196-1205.

[36] Y. Li, Y. Li, Y. Wan, Y. Xie, J. Zhu, H. Pan, X. Zheng, C. Xia, Perovskite oxyfluoride electrode enabling direct electrolyzing carbon dioxide with excellent electrochemical performances, Adv. Energy Mater. 9 (2019) 1803156.

[37] L. Jia, J. Gao, W. Fan, Q. Li. Carbon dioxide hydrogenation to methanol over the pre-reduced $LaCr_{0.5}Cu_{0.5}O_3$ catalyst. Catal Commun. 10 (2009) 2000-2003.

[38] E.-h. Yang, Y.-s. Noh, S. Ramesh, S. S. Lim, D. J. Moon. The effect of promoters in $La_{0.9}M_{0.1}Ni_{0.5}Fe_{0.5}O_3$ (M=Sr, Ca) perovskite catalysts on dry reforming of methane. Fuel Process.Technol. 134 (2015) 404-413.

[39] S. Park, Y. Kim, H. Han, Y.S. Chung, W. Yoon, J. Choia, W. B. Kim, In situ exsolved Co nanoparticles on Ruddlesden-Popper material as highly active catalyst for CO_2 electrolysis to CO, Appl. Catal. B 264 (2019) 147-156.

[40] Y. Kathiraser, Z. Wang, N.-T. Yang, S. Zahid, S. Kawi, Oxygen permeation and stability study of $La_{0.6}Sr_{0.4}Co_{0.8}Ga_{0.2}O_{3-\delta}$ (LSCG) hollow fiber membrane with exposure to CO_2, CH_4 and He, J. Membr. Sci. 427 (2013) 240-249.

[41] T. Yang, V. F. Mattick, Y. Chen, K. An, D. Ma, K. Huang, Crystal Structure and Transport Properties of Oxygen-Deficient Perovskite $Sr_{0.9}Y_{0.1}CoO_{3-\delta}$, ACS Appl. Energy Mater. 1 (2018) 822-832.

[42] J. Wang, T. Yang, L. Lei, K. Huang, Ta-Doped $SrCoO_{3-\delta}$ as a promising bifunctional oxygen electrode for reversible solid oxide fuel cells: a focused study on stability, J. Mater. Chem. A. 5 (2017) 8989-9002.

[43] J.-h. Myung, D. Neagu, D. N. Miller, J. T. Irvine, Switching on electrocatalytic activity in solid oxide cells, Nature. 537 (2016) 528-531.

[44] K. Chen, N. Li, N. Ai, Y. Cheng, W. D. Rickard, S. P. Jiang, Polarization-induced interface and Sr segregation of in situ assembled $La_{0.6}Sr_{0.4}Co_{0.2}Fe_{0.8}O_{3-\delta}$ electrodes on Y_2O_3–ZrO_2 electrolyte of solid oxide fuel cells, ACS Appl. Mater. Interfaces. 46 (2016) 31729-31737.

[45] S. Wang, H. Tsuruta, M. Asanuma, T. Ishihara, Ni–Fe–La(Sr)Fe(Mn)O_3 as a new active cermet cathode for intermediate - temperature CO_2 electrolysis using a $LaGaO_3$ - based electrolyte, Adv. Energy Mater. 5 (2015) 1401003.

Figure Captions

Fig. 1 XRD patterns (a) of as -synthesized LCaFN in air, treated with 5% H_2/N_2 and CO_2 at 800 °C for 5 h, H_2 -TPR curve (b), CO_2 -TPD curve (c), O_2-TPD curve (d), the conductivity (e) and TEC curve (f) of LCaFN.

Fig. 2 The morphology of LCaFN (a) R-LCaFN (b, c) and corresponding EDS mapping (d) and line scanning (d)

Fig. 3 High resolution TEM (a) and EDS-mapping (b) of LCaFN, high resolution TEM (c) and EDS-mapping (d) of R-LCaFN.

Fig. 4 I-V-P curve (a) and Impedance spectra (b), redox cycle stability test (c) and long-term stability test (d) of SSOC based on LCaFN-GDC electrode.

Fig. 5 I-V curves (a) and EIS (b) of the SSOC for pure CO_2 electrolysis at different temperatures. EIS of SSOC under different voltage (0~1.0 V) (c) and (1.2~2.0 V) (d) for CO_2 electrolysis at 800 °C.

Fig. 6 I-V curves (a) and EIS (b) of the SSOC for pure CO_2 electrolysis with switching the gas at 800 °C. EIS (c) of two modes at 1.4 V and long-term (d) test with switching the gas.

Fig. 7 XRD patterns (a) and Raman spectra (b) of both sides electrode, SEM images of whole cell (c), the SEM images of observed side (d) and reverse side (e), the magnified image reverse side (f) after long-term test.

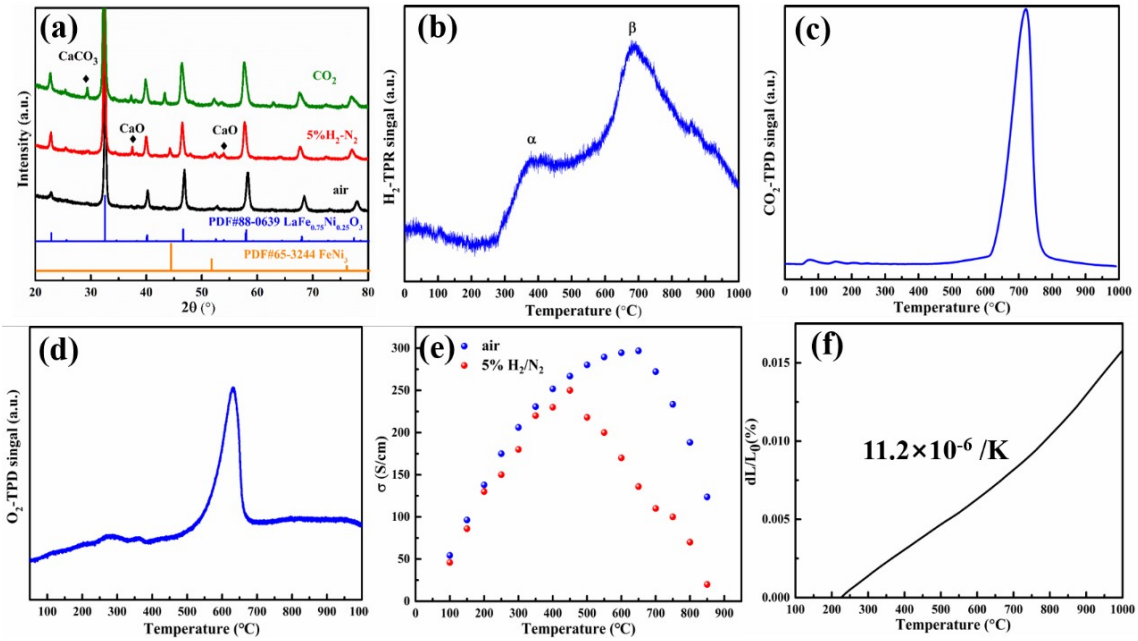

Fig. 1 XRD patterns (a) of as -synthesized LCaFN in air, treated with 5% H_2/N_2 and CO_2 at 800 °C for 5 h, H_2 -TPR curve (b), CO_2 -TPD curve (c), O_2-TPD curve (d), the conductivity (e) and TEC curve (f) of LCaFN.

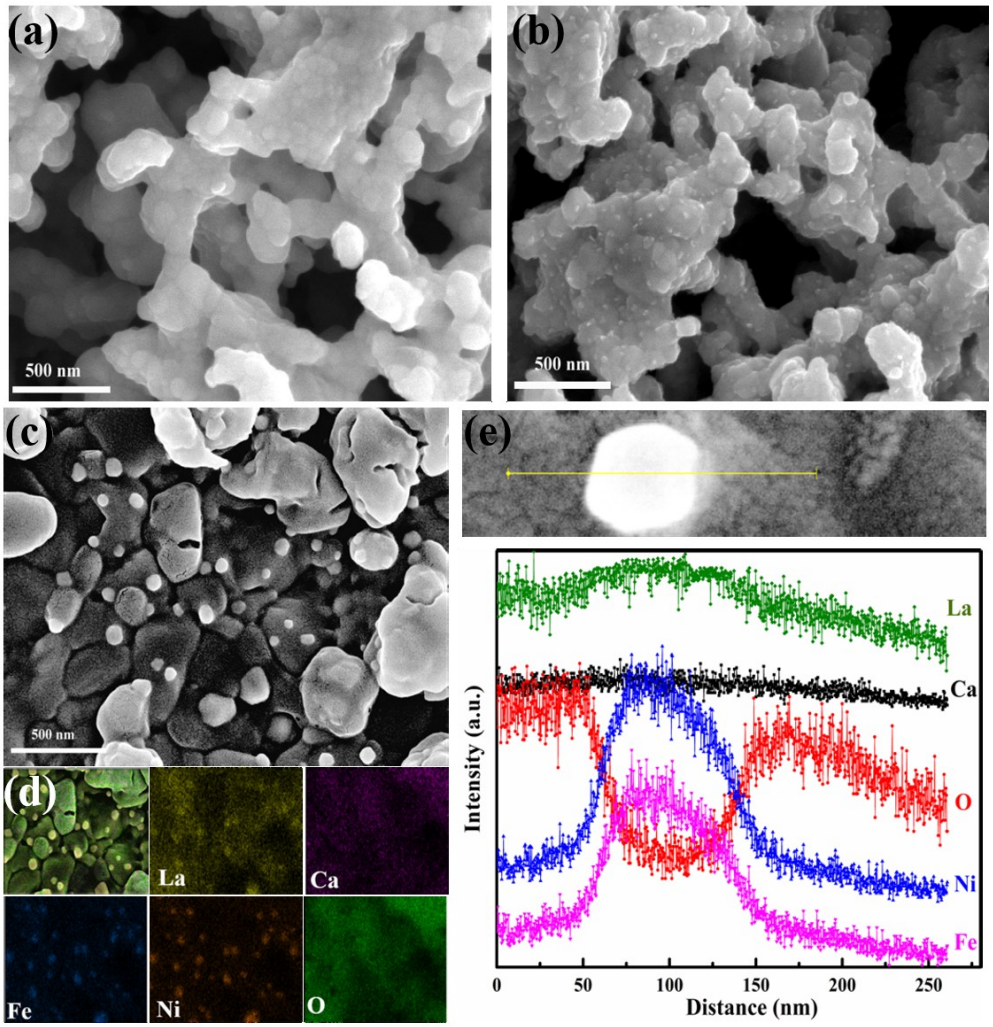

Fig. 2 The morphology of LCaFN (a) and R-LCaFN (b, c), corresponding EDS mapping (d) and line scanning (e).

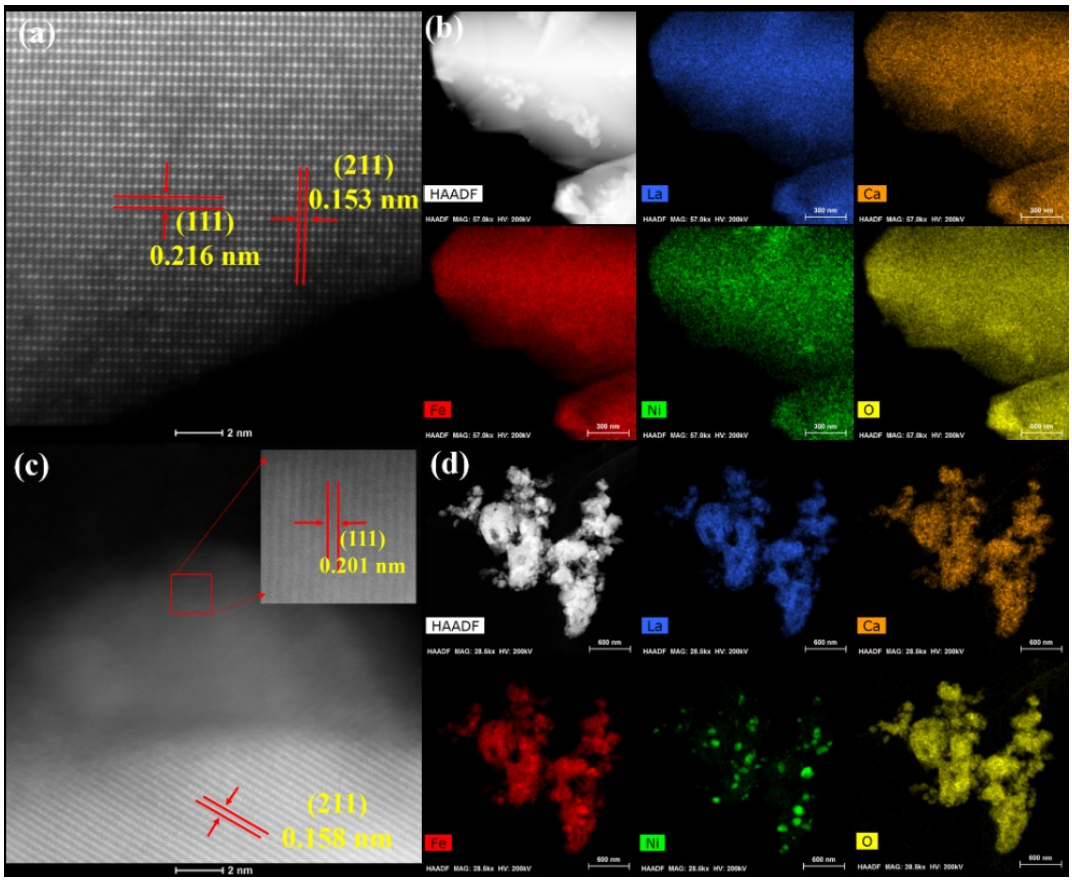

Fig. 3 High resolution TEM (a) and EDS-mapping (b) of LCaFN, high resolution TEM (c) and EDS-mapping (d) of R-LCaFN.

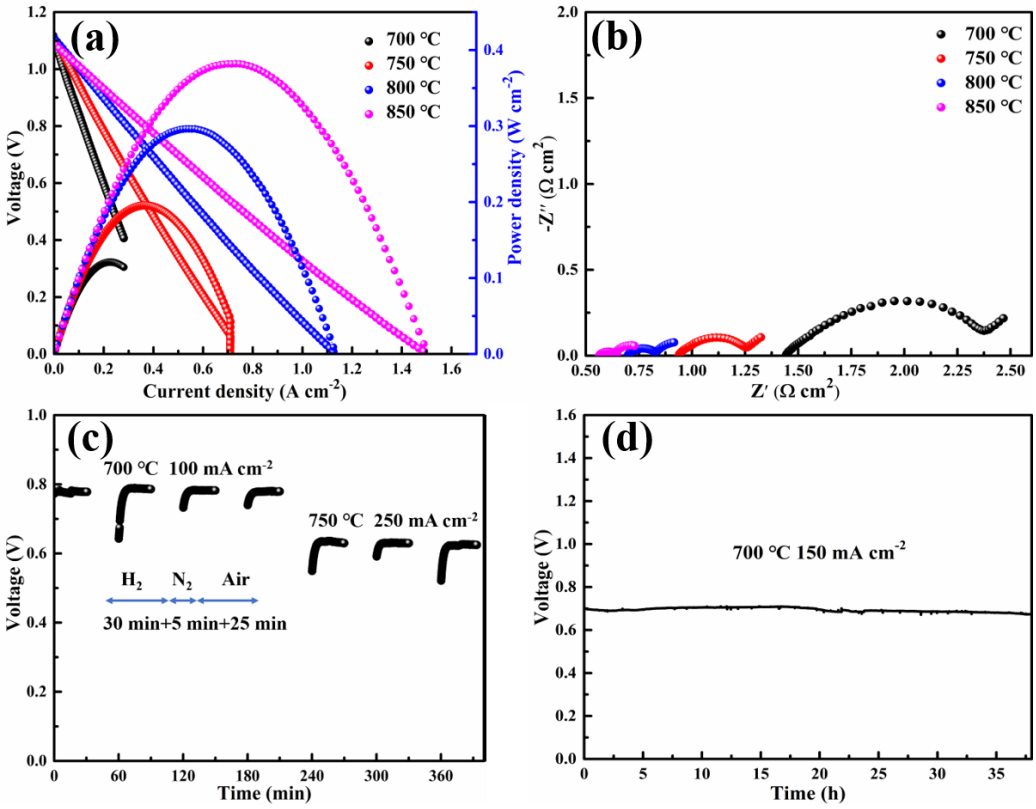

Fig. 4 I-V-P curve (a) and Impedance spectra (b), redox cycle stability test (c) and long-term stability test (d) of SSOC based on LCaFN-GDC electrode.

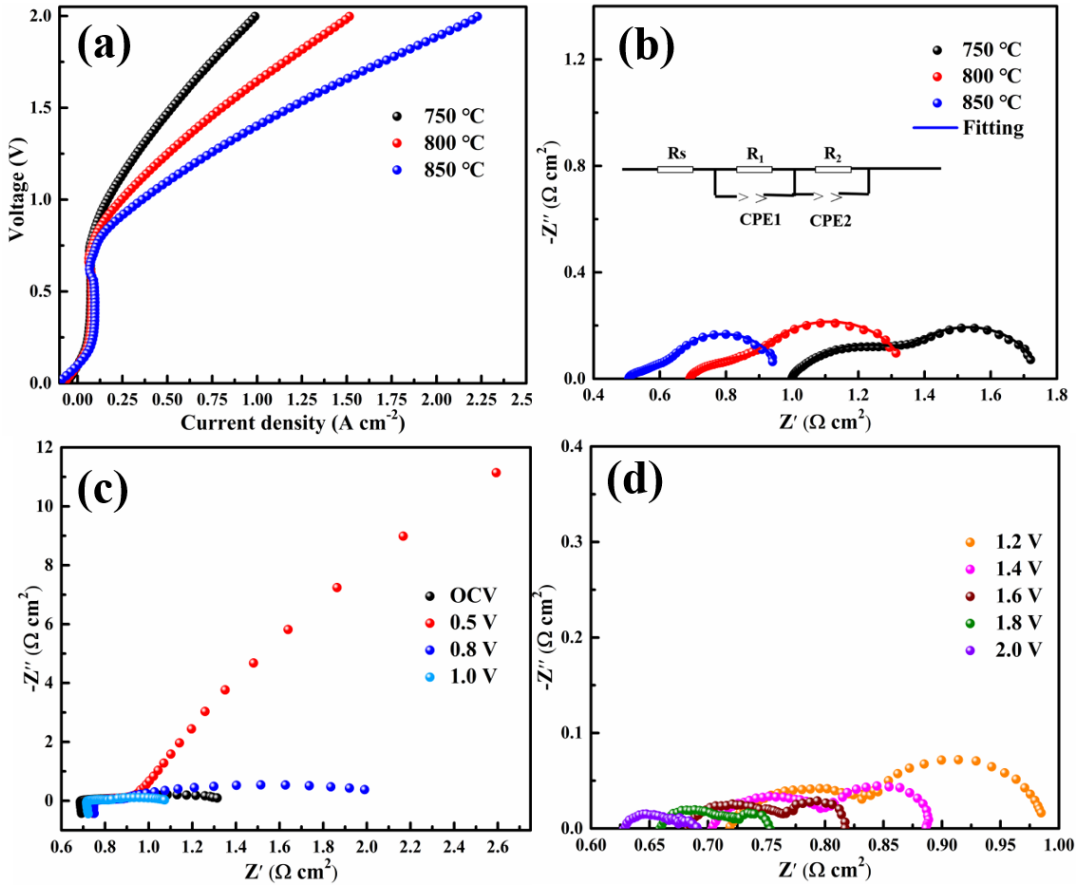

Fig. 5 I-V curves (a) and EIS (b) of the SSOC for pure CO_2 electrolysis at different temperatures. EIS of SSOC under different voltage (0~1.0 V) (c) and (1.2~2.0 V) (d) for CO_2 electrolysis at 800 °C.

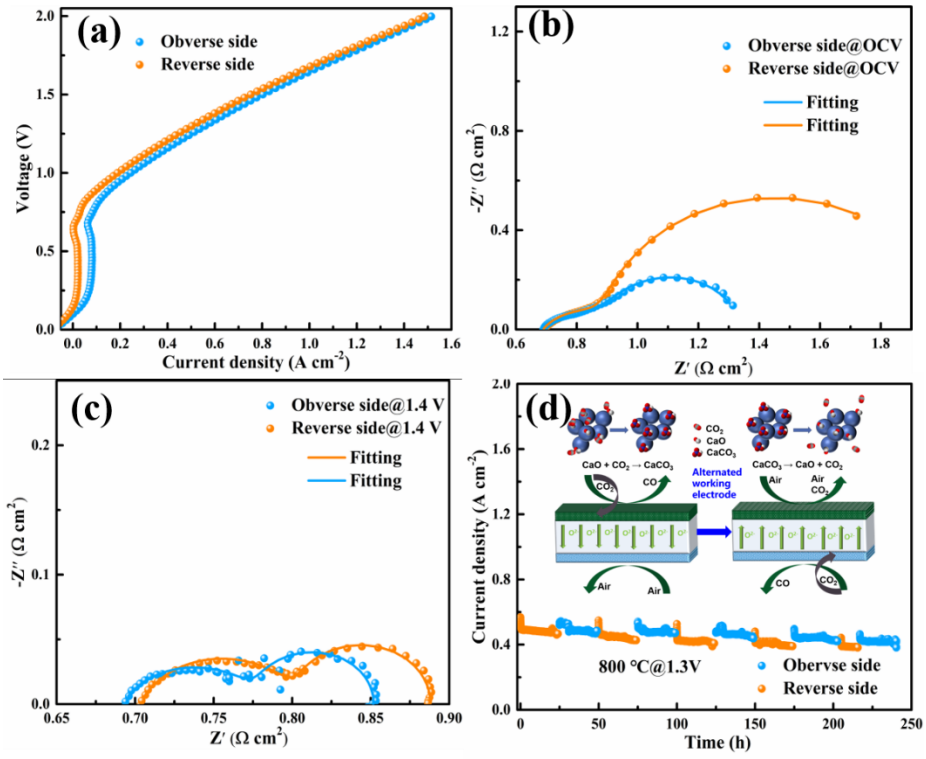

Fig. 6 I-V curves (a) and EIS (b) of the SSOC for pure CO_2 electrolysis with switching the gas at 800 °C. EIS (c) of two modes at 1.4 V and long-term (d) test with switching the gas.

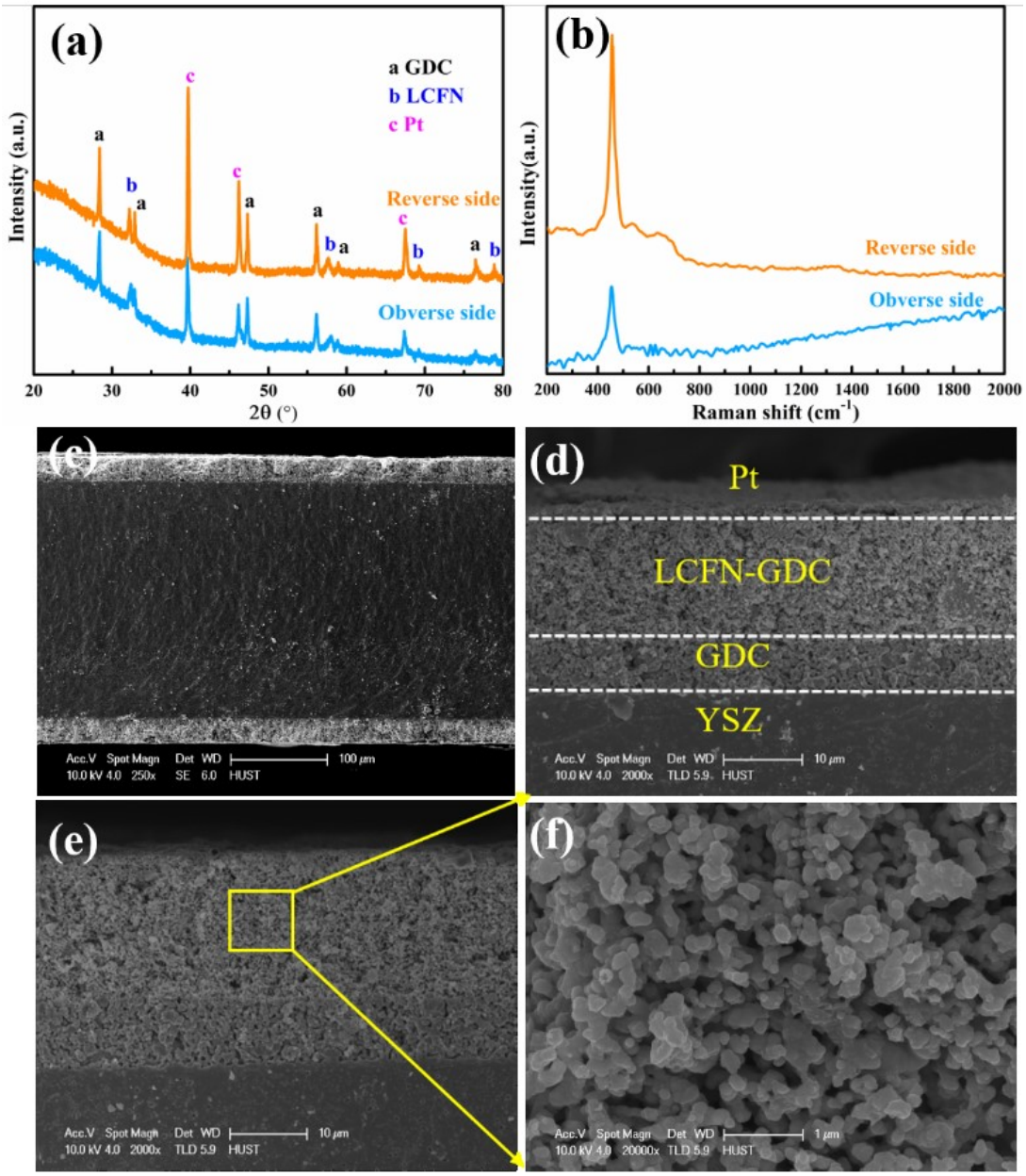

Fig. 7 XRD patterns (a) and Raman spectra (b) of both sides electrode, SEM images of whole cell (c), the SEM images of observed side (d) and reverse side (e), the magnified image reverse side (f) after long-term test.